JGP Journal of General Physiology

REVIEW

Voltage-Gated Na Channels 2026

Evolution of our understanding of the sodium channel fast inactivation: From Hodgkin and Huxley to the structural era

Yichen Liu[1], Cesar A. Amaya-Rodriguez[2,3], Victoria Collio[2], Gabriel Ibañez[2], Ramón Latorre[2], and Francisco Bezanilla[1,2,4]

Voltage-gated sodium (Nav) channels enable the rapid influx of sodium ions that are essential to generating the rising phase of the action potential. As originally described by Hodgkin and Huxley, once the Nav channel is activated, it switches to an inactivated state within milliseconds, a process they called inactivation. Internal perfusion of the giant axon of the squid with proteolytic enzymes eliminated inactivation, implying that the inactivation gate is an internal protein structure of the Nav channel. This result, together with the charge immobilization of the gating currents, led to the ball and chain model of inactivation. Deletion of the linker between domains III and IV of the four homologous domains of the Nav channel was found to remove fast inactivation. These observations evolved the ball and chain model to the hinged-lid model of fast inactivation, which dominated the field for nearly 30 years. Surprisingly, the structures of the Nav channel, determined by cryo-EM, showed that the IFM was not at the site predicted by the hinged-lid model. Upending the Na channel field, biophysical and mutagenesis studies revealed that the binding of the IFM motif allosterically closes an inactivation gate at the internal entrance of the Nav conduction system. In this Review, we compile the historical and structural evolution of the fast inactivation process, from the first functional descriptions to current models based on structural data.

Introduction

The initiation and conduction of action potentials in excitable tissues such as neurons, axons, heart, and skeletal muscles rely on voltage-gated sodium (Nav) channels. Nav channels are a family of specialized membrane proteins expressed ubiquitously in excitable tissues and play fundamental roles in our physiology. Functionally, Nav channels open (activate) in response to depolarization of the membrane potential from its negative resting potential. Opening of the Nav channels allows inward Na^+ ion flux, which further depolarizes the membrane and activates additional Nav channels, generating the fast upstroke of the action potential. Thus, the Nav channels operate via positive feedback, and, as with all positive feedback systems, an inhibitory mechanism is necessary to recover the original state, here, the membrane potential. At the cellular level, this is normally achieved by a delayed turn-on of a voltage-gated potassium (Kv) current or by the passive membrane leakage. But if the Nav channels were still open, the outward K^+ current may not be large enough to be net outward, and a plateau potential would develop. Therefore, at the molecular level, another mechanism exists. A few milliseconds after activation, Nav channels rapidly enter a nonconductive state: the fast-inactivated state. Fast inactivation is the autoinhibitory switch that attenuates Na^+ conductance, allowing the membrane potential to reset after a brief transient depolarization: the action potential. Therefore, fast inactivation plays essential roles in our physiology, and, unsurprisingly, abnormalities in fast inactivation have been associated with a wide range of diseases manifesting in diverse tissues.

In this Review, we will discuss the molecular mechanism of fast inactivation in Nav channels. Given how the view of Nav channel fast inactivation mechanisms have evolved, it would be of interest to the reader to take a historical approach, from the "*h*" term in the Hodgkin and Huxley model (Hodgkin and Huxley, 1952c; Hodgkin and Huxley, 1952d) to the "ball and chain" model (Bezanilla and Armstrong, 1977) and later the modified "hinged-lid" model (West et al., 1992). We will discuss the results of key early experiments that led to these conceptual advancements through 2018, at which point it was widely

[1]Department of Biochemistry and Molecular Biology, University of Chicago, Chicago, IL, USA; [2]Centro Interdisciplinario de Neurociencia de Valparaíso, Facultad de Ciencias, Universidad de Valparaíso, Valparaíso, Chile; [3]Departamento de Fisiología y Comportamiento Animal, Facultad de Ciencias Naturales, Exactas y Tecnología, Universidad de Panamá, Ciudad de Panamá, Panamá; [4]Facultad de Ciencias del Mar y Recursos Naturales, Universidad de Valparaíso, Valparaíso, Chile.

Correspondence to Francisco Bezanilla: fbezanilla@uchicago.edu; Ramón Latorre: Ramon.Latorre@uv.cl.

believed that the mechanism of fast inactivation was largely a solved problem. However, with the development of cryo-EM, the first protein structure of a mammalian Nav was solved, unexpectedly revealing that the inactivating particle was not where it was predicted to be in the inactivated Nav channel by the existing model (Pan et al., 2018). We will address the apparent discrepancy between the available structural data and the canonical model and discuss recent attempts to reconcile the functional and structural results. During the process, we will revisit early studies, comparing and reinterpreting their results in light of subsequent structural data. Finally, we will propose a new theoretical framework to describe the inactivation process and discuss the open questions regarding fast inactivation within the latest model.

From the *h* term to the ball and chain model

The first description of fast inactivation: The "*h* term"

Fast inactivation was first described by Hodgkin and Huxley in their seminal 1952 series of papers (Hodgkin et al., 1952; Hodgkin and Huxley, 1952a; Hodgkin and Huxley, 1952b; Hodgkin and Huxley, 1952c; Hodgkin and Huxley, 1952d). Depolarization of the membrane potential activates sodium conductance, albeit with a short delay, which was explained by assuming the existence of three (m) independent activating particles; hence, activation was described using an m^3 term representing the probability of being open, which depends on voltage and time (Hodgkin and Huxley, 1952d). Membrane depolarization also attenuates the sodium permeability soon after activation in a voltage-dependent manner, an "inactivation" process (Hodgkin and Huxley 1952c). This process decays exponentially in time, seemingly concurrently with the activation (the m^3 term) process upon depolarization. Hodgkin and Huxley (1952d) introduced an h term (the probability of not being inactivated) to obtain a complete description of the sodium conductance (g_{Na}) as a function of voltage and time.

$$g_{Na} = m^3 h \overline{g_{Na}}$$

where $\overline{g_{Na}}$ is the maximum g_{Na}.

Discussing the possible mechanism of this fast inactivation process, Hodgkin and Huxley (1952d) proposed: "inactivation might be due to the movement of a negatively charged particle which blocks the flow of sodium ions when it reaches the inside of the membrane." This ingenious remark predicted the existence of an "inactivation particle," a concept that is still widely used today and paved the way for the classical ball and chain model for fast inactivation.

Evidence of protein origin of inactivation

Following Rojas and Luxoro's early attempts, who showed that axon excitability was destroyed when the axon was injected with a protease (Rojas and Luxoro, 1963), Armstrong et al. (1973) discovered that pronase, a non-specific protease, could remove fast inactivation of the sodium conductance when perfused internally in the giant squid axon (Fig. 1 A). Interestingly, the removal of fast inactivation did not impede the voltage-dependent activation of sodium conductance. It seemed that activation and fast inactivation relied on two separate gating mechanisms and that a proteinaceous, intracellular component was responsible for fast inactivation.

A comparison of the WT, fast-inactivating Na^+ current and pronase-treated non-inactivating Na^+ current revealed that, instead of occurring concurrently with activation as predicted by the HH model, fast inactivation had a delayed onset (On) (Armstrong and Bezanilla, 1977). It appeared that for fast inactivation to proceed, some degree of activation was required (Bezanilla and Armstrong, 1977), which contrasts with the m^3h formulation that posits that h changes independently of m and, as it is a two-state process, starts decaying concurrently with membrane depolarization.

Voltage dependence of inactivation

Both activation and inactivation are voltage dependent, meaning that the Nav channel should exhibit gating currents, due to the transient movement of the voltage sensors, for both processes. Gating currents were predicted by Hodgkin and Huxley when referring to the origin of the voltage dependence: "the changes in ionic permeability depend on the movement of some component of the membrane which behaves as though it had a large charge or dipole moment" (Hodgkin and Huxley, 1952d). It was found that the kinetics of the onset of (On) gating currents exhibit two kinetics components: a fast component related to the channel activation and a slow component that is slower than activation but faster than inactivation (Armstrong and Bezanilla, 1977). Although no gating-current component showed fast inactivation kinetics, the movement of the voltage sensors, as detected by gating-current measurements, was hindered by fast inactivation. This effect was observed when recording the gating current at the offset (Off) of a depolarizing voltage pulse of different durations, which ended with repolarization of the membrane to −140 mV.

As fast inactivation progressed, the gating current at the Off of the pulse showed a slow component (see Fig. 1 B). The area under the slow component (the charge) increased, while the area under the fast component decreased as the pulse was prolonged; the time course of these changes followed the time course of the inactivation of the ionic current (Armstrong and Bezanilla, 1977). The kinetics of the slow component of the Off-gating current exhibited the voltage dependence and time course of the recovery of inactivation of the ionic current. As Hodgkin and Huxley (1952c) showed, the recovery from inactivation becomes slower at less hyperpolarized potentials, so that when the membrane depolarization was returned to a voltage, like −70 mV (instead of −140 mV), the slow component of the gating charge was so slow that it became undetectable, showing a decrease in the total charge at the Off as inactivation is settled.

Of course, the Off charge must be equal to the On charge, so the fact that it is measured to be smaller just indicates that it was not detected at that voltage; only when the Off-gating current was faster, at −140 mV or at warmer temperature, could all the charge be detected. This apparent decrease in charge is the origin of the term "charge immobilization". Around 60% of the total gating charge became immobilized as fast inactivation progressed and would only return to the resting state upon

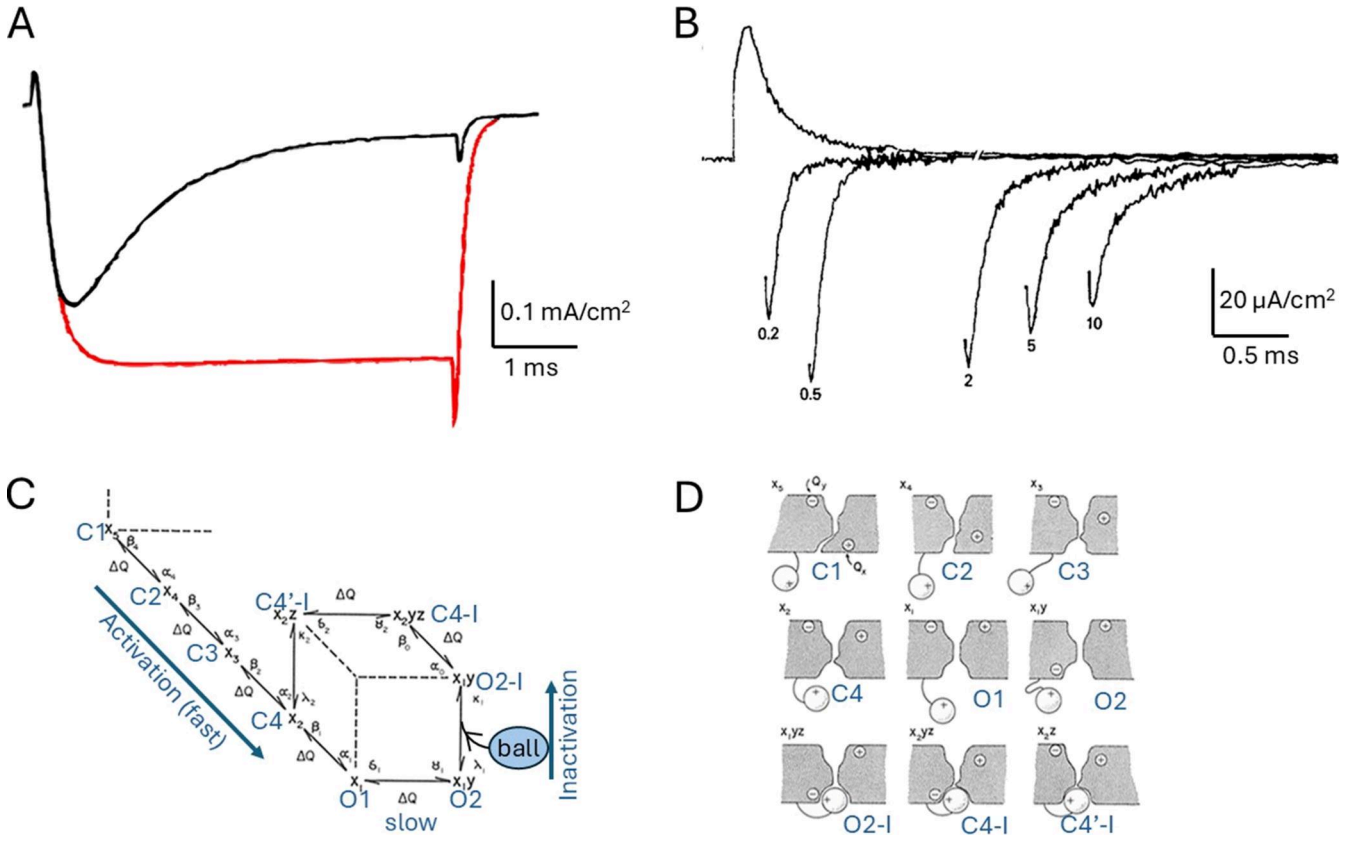

Figure 1. **Origins of the Ball and Chain model of fast inactivation. (A)** Sodium current of squid giant axon before (black) and after pronase treatment (red) for a depolarization to 0 mV from a holding potential of −70 mV. The initial outward current is a gating current observed because the external solution contained 1/5 sodium (modified from Stimers et al., 1985). **(B)** Gating current for a depolarization to 0 mV from −140 mV, showing the off current for different pulse durations as indicated, returning to −140 mV (modified from Armstrong and Bezanilla, 1977). **(C and D)** Model of activation and inactivation that introduced the ball and chain model (modified from Armstrong and Bezanilla, 1977).

recovery from fast inactivation. To explain their observations, Armstrong and Bezanilla (1977) envisioned a charged inactivation particle, a "ball," tethered by a flexible linker, a "chain," close to the permeating pathway in the intracellular side of the membrane (Fig. 1, C and D). Upon membrane depolarization, there is a fast and slow movement among the voltage sensors. The fast component is permissive for channel opening, and the slow component is required for the inactivation particle to bind to the mouth of the channel (the second slower component of the gating current) (Fig. 1 C), thus blocking the pore (inactivation) and immobilizing the voltage sensor.

To recover from inactivation, some activation charge must move back to allow the ball to unbind, thus unblocking the channel after the activation gate has closed, explaining why, upon repolarization, there is no ionic current (Armstrong and Croop, 1982). In this context, pronase would simply clip off the ball, removing inactivation. As such, the canonical ball and chain model for fast inactivation was formulated. In this model, since the actual closure of the inactivation gate is the ball blocking the pore, it is not expected to be very voltage dependent. This prediction is in agreement with the single channel recordings on neuroblastoma cells by Aldrich et al. (1983) and the kinetic modeling of the sodium channel resulting from the fit of data from single channels, macroscopic ionic, and gating currents of the squid giant axon (Vandenberg and Bezanilla, 1991).

Cloning of the first Nav channel and identification of the inactivation particle

While it is now common knowledge that specialized ion channels in the cell membrane regulate the passage of ions across the membrane, in Hodgkin and Huxley's time, the idea of a pore-forming channel was not considered. However, in their last paper, Hodgkin and Huxley (1952d) did predict the existence of discrete channels when they discussed the movement of charges and dipoles of the voltage sensor that were too small for them to detect: "if such components exist" (charge or dipole moment) "it is necessary to suppose that their density is relatively low and that a number of sodium ions cross the membrane at a single active patch."

Even though the K^+ flux ratio experiments gave the first hint that the ionic conductance of the giant squid axon came from pores or channels on the membrane (Hodgkin and Keynes, 1955), the existence of ion channels as specialized membrane proteins was only demonstrated years later through biochemical and electrophysiological investigations (Hille, 1970; Hille, 1971; Hille, 1973; Armstrong et al., 1973; Neher and Sakmann, 1976). Taking

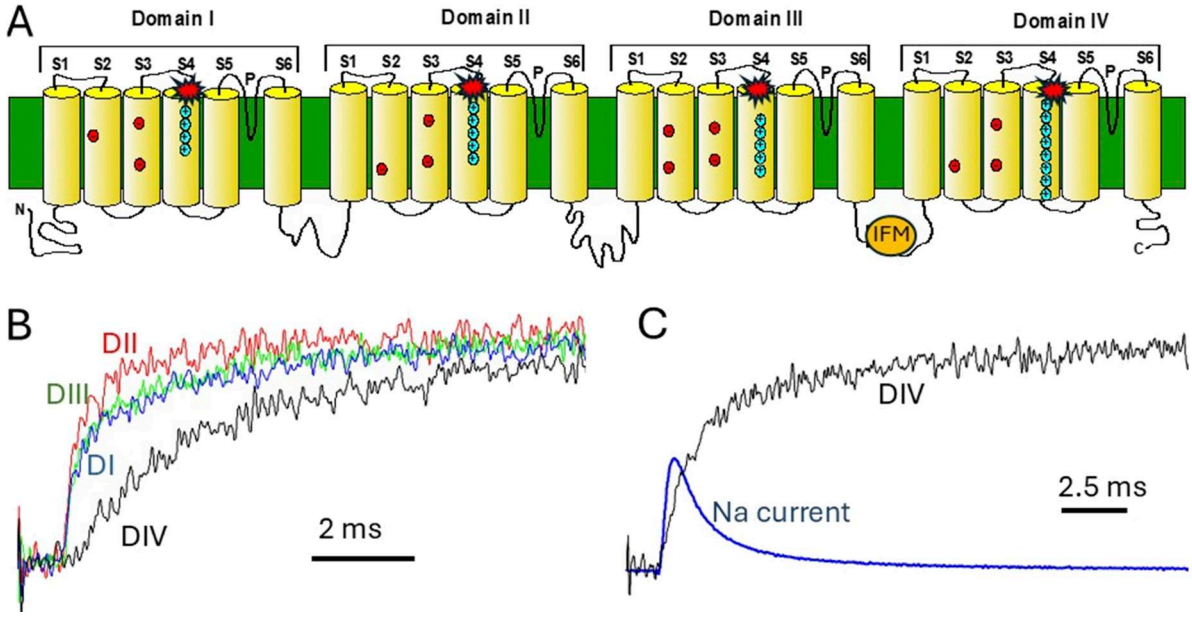

Figure 2. **Voltage sensor dynamics and the hinged-lid model of fast inactivation. (A)** Secondary structure of Nav1.4 showing the four domains and the six transmembrane segments of each domain. The stars indicate the positions of the fluorophores used to follow the conformational changes of the VSDs. **(B)** Fluorescence signals of domains I–IV as indicated for a pulse to −10 mV. Notice how slow DIV is compared with the other domains. **(C)** Comparison of the fluorescence signal of DIV with the sodium current in reverse gradient for a depolarization to −10 mV, showing that the sodium current precedes the movement of VSD of DIV. (C and D modified from Chanda and Bezanilla, 2002).

advantage of the electrocytes that express a high density of Nav channels from the electric eel and the high affinity of the Na^+ channel for TTX, Agnew and colleagues were able to extract and purify a 230-kDa protein (Agnew et al., 1978), illustrating the protein nature of the Na^+ channel. This protein was later found to conduct Na^+ in liposomes and, subsequently, demonstrated to induce Na^+ channel currents in liposomes and bilayers (Rosenberg et al., 1984; Correa et al., 1990).

One of the final confirmations of the channel theory was provided by Numa's group in the 1980s when they cloned the Nav channel from the electric eel (Noda et al., 1984). Subsequently, other Na^+ channels were cloned, and the sodium conductance was recreated by expressing the protein in a heterologous system (Noda et al., 1984; Noda et al., 1986). From that time, our understanding of ion channels has entered the molecular era.

At the molecular level, Nav channels, at least in eukaryotes, have a pseudo-tetrameric arrangement. The channels comprise four domains (DI–DIV), each with six transmembrane segments (S1–S6), connected by flexible linkers. The transmembrane segments S1–S4 form the voltage-sensing domain (VSD) with positively charged amino acids in S4 serving as gating charges. The permeation pathway is formed by the pore domain, which consists of segments S5 and S6, with loops between S5 and S6 constituting an asymmetric selectivity filter (SF) (Fig. 2 A).

With the molecular structure of the Nav channel elucidated, the search for the fast inactivation particle began. The first hint of the molecular identity of the inactivation particle came in the late 1980s. The Catterall group demonstrated that antibodies directed against the intracellular linker between the DIII and DIV domains blocked Nav channel inactivation in rat muscle cells, indicating a direct involvement of this region in the process (Vassilev et al., 1988). In a complementary approach, Stühmer et al. (1989) split the DNA of the Nav channel into two fragments at the DIII–DIV linker by restriction enzyme digestion. The split channel constructs, when co-expressed, allowed for a persistent Na^+ current with slowed inactivation. Clearly, the inactivation particle must exist in the DIII–DIV linker. West et al. (1992) conducted a series of mutagenesis experiments on the hydrophobic residues in the linker. They discovered an amino acid trio, isoleucine, phenylalanine, and methionine, which came to be known as "the IFM motif" and which was necessary for fast inactivation (Fig. 2 A). Replacing the IFM motif with triple glutamine, the QQQ mutant, led to non-inactivating channels. Furthermore, fast inactivation could be restored by perfusing a short, minimal pentapeptide "KIFMK," which mimics the IFM motif, into the QQQ mutant. This result seemed to prove the motif´s ability to block the pore directly, though closer examination of this result later in the review will reveal some caveats. Collectively, this series of observations led to the revised hinged-lid model. In this view, the fast inactivation particle was identified to be no longer the charged particle originally envisioned but a hydrophobic "lid" that "hinged" between DIII and DIV. Similarly, when the channel opens, the lid would close, blocking the permeation pathway and leading to fast inactivation.

Specialized role of DIV VSD in fast inactivation

Across the animal kingdom, ion channel toxins are used as predatory as well as defense mechanisms, and researchers realized very early on that these toxins could serve as natural molecular probes for ion channel studies (Stevens et al., 2011). α scorpion toxins and sea anemone toxin II were shown to modify

fast inactivation in Nav channels directly. (Rogers et al., 1996; Ulbricht, 2005; Stevens et al., 2011). When applied externally, these toxins can significantly slow down the Nav channel inactivation kinetics. Interestingly, in addition to ionic currents, these toxins can also modify gating currents: toxin binding decreases total gating charges and largely eliminates the slow component of the gating current (Hanck and Sheets, 2006; Campos et al., 2008). The dual effects of the toxins were better understood in the late 1990s, when the Catterall group identified their binding site. Now categorized as site 3 toxins, both α scorpion toxins and ATX-II have a conserved binding site in the external S3–S4 loop of DIV VSD, and the toxins appear to slow/stop DIV VSD activation (Rogers et al., 1996). Thus, it seems that DIV VSD plays a specialized role in fast inactivation, and perhaps for fast inactivation to occur, DIV VSD must be in the active state, which could also explain the delayed On of fast inactivation.

At the same time, the first direct measurements of VSD movements in Nav channels were made possible by the newly developed site-directed voltage-clamp fluorimetry technique (Mannuzzu et al., 1996; Cha and Bezanilla, 1997; Cha and Bezanilla, 1998). By conjugating quenchable fluorophores to sites available from the extracellular solution of different voltage sensors, local sensor movements were detected as changes in the fluorescence readouts. Then, by controlling the site of conjugation, VSD movements of each domain of Nav channels could be studied individually. First, Cha et al. (1999) observed that DIII VSD and DIV VSD were both immobilized during fast inactivation, whereas DI and DII VSDs moved unimpededly. Second, Chanda and Bezanilla (2002) measured the movement of each S4 segment concomitantly with gating currents or ionic currents during activation and inactivation. The movements of DIV VSD were distinct, activating significantly more slowly than the other VSDs (Fig. 2 B), thereby manifesting as the slow component in the gating current. Moreover, the kinetics of DIV VSD movements were even slower than the activation of ionic current (Fig. 2 C) and instead closely but not exactly followed the development of fast inactivation. Third, charge-neutralization experiments immobilized DIV VSD in a likely active state and demonstrated that DIV VSD activation was both sufficient and necessary for the development of fast inactivation (Capes et al., 2013). As such, it became widely accepted that DIV VSD had a specialized role, and its activation was required for fast inactivation to occur.

The resolution revolution and the first mammalian Nav channel structure

Before discussing the protein structural results, it is worth summarizing the classical model for fast inactivation up until that point. The canonical model predicted that upon depolarization, DIV VSD activation, which occurred more slowly than the On of the ionic current, facilitated the progression of fast inactivation, likely by exposing a binding pocket for the IFM motif at the intracellular end of the permeation pathway. Once exposed, the IFM motif would then wedge inside the pore and block the Na^+ conductance. Meanwhile, binding of the IFM motif would immobilize the VSDs in DIII and DIV, possibly through hydrophobic interactions, and their mobility would be restored only after the inactivation particle was unbound, leading to recovery of fast inactivation.

In 2017, Yan's group solved the first vertebrate Nav channel structure from the electric eel. Subsequently, in 2018, the first mammalian Nav channel structure was finally solved in a putative fast-inactivated state utilizing the improved single-particle cryo-EM technique (Yan et al., 2017; Pan et al., 2018). Surprisingly, these structures revealed that the IFM motif (LFM motif in the electric eel case), rather than directly occluding the pore as previously proposed, was inserted into a hydrophobic pocket located away from the pore. This result directly challenged the classical notion that the motif functions as the inactivation gate (Fig. 3 A). Since then, numerous structural studies of various isoforms of Nav channels have confirmed the original observation that the IFM motif does not block the pore in the fast-inactivated state (Pan et al., 2018; Jiang et al., 2020; Jiang et al., 2021; Zhang et al., 2022). While the IFM motif is unquestionably necessary for fast inactivation, the protein segment does not occlude the pore itself. Instead, it must trigger some changes at the pore that renders the channel nonconductive. Clearly, the classical model could no longer explain the new experimental results, and a new theoretical framework was required.

Identification of an S6-located fast inactivation gate

The most obvious discrepancy between the structural results and the canonical model is the identity of the fast inactivation gate. While the canonical model predicts that the IFM motif directly blocks the pore, structural data argue otherwise (Fig. 3 A). To address this discrepancy, the Bezanilla group reanalyzed the available structural data and identified a two-layered hydrophobic barrier that formed the narrowest part of the pore in the inactivated state (Liu et al., 2023). This two-layered hydrophobic barrier comprises eight hydrophobic residues in total, two from each domain. Moreover, within the S6 of each domain, the two residues were one α helical turn away from each other. In DIII and DIV, those residues were bulky and hydrophobic, leucine or isoleucine. Reducing the size by single alanine replacement of the large hydrophobic residues yielded little change to fast inactivation. However, when both residues in the same domain were mutated to alanine, either in domain III (DIIIAA mutant) or in domain IV (DIVAA mutant), significant steady-state current was observed (Fig. 3 C), indicating that the channels' ability to enter a nonconducting inactivated state was diminished, or, conversely, that the inactivated state had become conducting.

While numerous mutants with incomplete fast inactivation exist in the literature, DIIIAA and DIVAA behaved very differently from those mutants. Typically, incomplete fast inactivation is caused by a reduced free-energy difference between the open- and fast-inactivated states, allowing a subpopulation of channels to remain in (or repeatedly reenter) open state during depolarization. This is not the case for DIIIAA or DIVAA mutants.

The steady-state current observed in the mutants was conducted not through the open state but rather through an

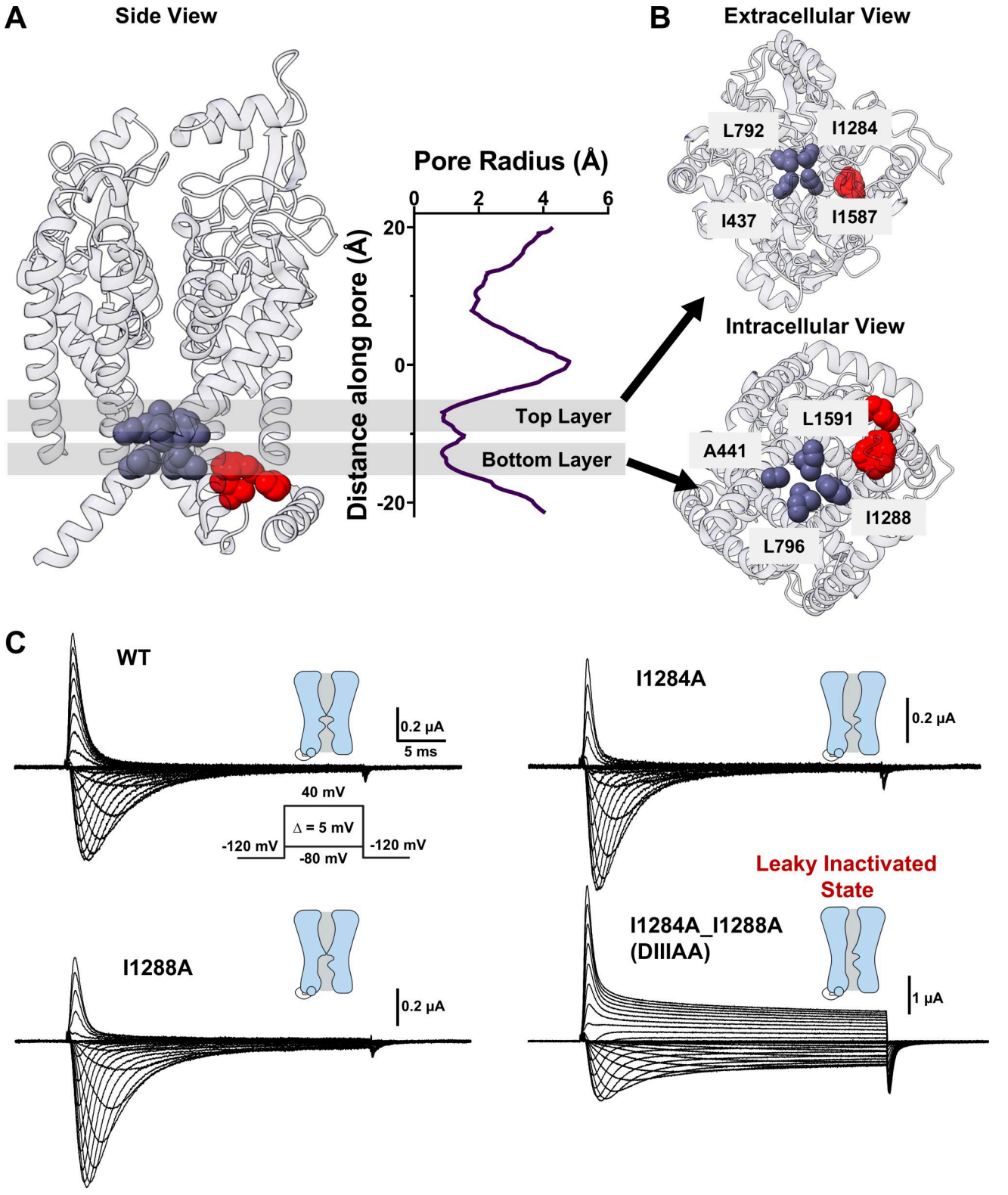

Figure 3. **Structural identification of the hydrophobic gate underlying fast inactivation. (A)** View of the position of the hydrophobic gate residues in the pore of the sodium channel (in dark blue) and the location of the IFM motif (in red). Numbering is based on rNav1.4. **(B)** Pore radius along the length of the pore, indicating the narrowing where the two layers of hydrophobic residues reside. Residue numbers are named from rNav1.4 (modified from Liu et al., 2023). **(C)** Effects on ionic currents of mutations of the gate residues on ionic traces. For simplicity, only domain III is shown. Ionic currents families are shown for WT, the two DIII single alanine mutations (I284A and I288A), and the double alanine mutation, named DIIIAA. Only when both residues were mutated simultaneously was a steady-state current observed through the leaky inactivated state, as indicated by the cartoons next to the current traces (modified from Liu et al., 2023).

alternative conductive state. Several lines of evidence supported this notion. If all channels are equally affected by a particular mutation, as is the case here, incomplete inactivation is expected to slow down the kinetics of the residual inactivation. In contrast, in DIIIAA, the residual fast inactivation kinetics remained similar to the WT channels. Additionally, the deactivation kinetics changed as a function of depolarization time and followed the same kinetics as the apparent fast inactivation development. More surprisingly, the relative in selectivity between Na^+ and K^+ also changed concurrently with the development of fast inactivation.

All these results are consistent with the view that in DIIIAA and DIVAA, as fast inactivation proceeds, the channels transition from the open state to a different conductive state with slower deactivation kinetics and decreased selectivity for Na^+ ions: a leaky inactivated state due to the reduced size (alanine) of the hydrophobic barrier (leucine and isoleucine). In addition, while both DIIIAA and DIVAA showed incomplete inactivation of ionic current, gating-charge immobilization analysis painted a different picture. Despite the significant steady-state current in both DIIIAA and DIVAA, gating charge immobilization progressed at the same rate and to the same degree as in WT, with ~60% of immobilized total gating charge, meaning that the channels entered the fast-inactivated state but remained conductive. Based on these observations, Liu et al. (2023) proposed that the identified large hydrophobic amino acid residues in DIII and DIV S6 work together as the fast inactivation gate. Reducing the volume of these residues, while not hindering entry into the fast-inactivated state, leaves the final fast-inactivated state still conductive and creates a "leaky" inactivated state.

In retrospect, the results from DIIIAA and DIVAA should not come as a surprise. Numerous studies have previously demonstrated the importance of the S6 region for fast inactivation. Batrachotoxin, a site-2 toxin from the poison dart frog, binds to the intracellular ends of the S6 helices and can remove fast inactivation entirely (Correa et al., 1991; Tonggu et al., 2024). In addition, mutagenesis experiments have pointed out the importance of this region. The Catterall group conducted a thorough alanine-scanning survey of the S6 helices from all four domains (Yarov-Yarovoy et al., 2002) and revealed the contribution of S6 residues to the fast inactivation process. Likewise, Wang group identified a combination of DI S6 mutations that could remove most of the fast inactivation (Wang et al., 2003). However, these physiological results were interpreted within the framework of the canonical ball and chain or hinged-lid models. The identified residues were hypothesized to be part of the binding site for the IFM motif rather than the gate itself. Considering that the double-layered hydrophobic residues work together, meaning that both residues in each S6 must be modified to manifest a change in fast inactivation, it would be difficult for those previous single mutant studies to uncover the nature of the inactivation gate.

The IFM motif as a coupler between DIV VSD and inactivation gate

In the canonical model, the IFM motif is predicted to be a direct pore blocker, and the inactivation KFIMK peptide experiments appeared to have provided evidence supporting this notion (Eaholtz et al., 1994). However, it is worth pointing out that the inactivation peptide behaved more like an open-channel blocker, as was demonstrated later by Tang, Kallen, and Horn in 1996 (Tang et al., 1996), resembling the N-type inactivation observed in Kv channels (Hoshi et al., 1990). The peptide-inhibited channels showed increased tail currents upon repolarization, which is never the case in WT channels (Armstrong and Croop, 1982; Kuo and Bean, 1994; Aman and Raman, 2024), and slowed deactivation kinetics, a phenomenon best described by a "foot in the door" mechanism in which the inhibitor inserts into the open channel and channel closure is only possible upon disinhibition (Armstrong, 1971). With this mechanism, however, it is difficult to explain the closed-state inactivation observed on Nav channels (Armstrong, 2006). Additionally, studies have shown that the Nav inactivation peptide blocks the chimeric potassium channel (Patton et al., 1993) and restores fast inactivation in fast inactivation–deficient mutants where the native IFM motif remains intact (Wang and Wang, 2005). In the presence of the structural evidence and DIIIAA/DIVAA results, the inactivation peptide should probably be more accurately reinterpreted as a less selective open channel blocker that functions in a different way from the IFM motif.

Even though the IFM motif does not serve as the pore-blocking inactivation gate, studies have repeatedly demonstrated the importance of the IFM motif in fast inactivation. Now, with the identification of an S6-located inactivation gate, what is the role of the IFM motif? Recent site-directed voltage-clamp fluorimetry experiments using the unnatural amino acid ANAP provided insights into this question (Liu et al., 2025). ANAP is a fluorescent unnatural amino acid (Chatterjee et al., 2013) that is structurally similar to PRODAN (Weber and Farris, 1979) and only slightly larger than tryptophan. Its fluorescence depends on the hydrophobicity of its local environment, making it a good reporter for conformational changes. By incorporating ANAP into key regions of the Nav channels and monitoring changes in the fluorescence signal, it is possible to record conformational changes during fast inactivation while simultaneously measuring function, either with ionic or gating currents. Three regions were monitored: the IFM motif, the DIII–DIV linker, where the IFM is located, and the intracellular end of DIII S6.

At the DIII–DIV linker, a single, fast movement was observed upon depolarization. The kinetics of this movement were faster than the development of fast inactivation (Fig. 4, A and B) but followed the kinetics of the slow component of the gating current, manifested by the movement of the VSD (S4) of domain IV (Fig.4 A). However, movement at the IFM motif during inactivation was quite different. Substituting the IFM motif with I_ANAP_M revealed a composite fluorescence signal: a fast component that was faster than the inactivation of the ionic current but was like the linker movement and a slow component that followed the development of inactivation (Fig. 4 C). Finally, near the most intracellular part of the S6 of DIII, a slow fluorescence signal was detected, following the closure of the inactivation gate with a delayed On, like what was observed in the pronase experiments (Fig.4 D). Based on these observations, the fast inactivation process can be described schematically, as shown in

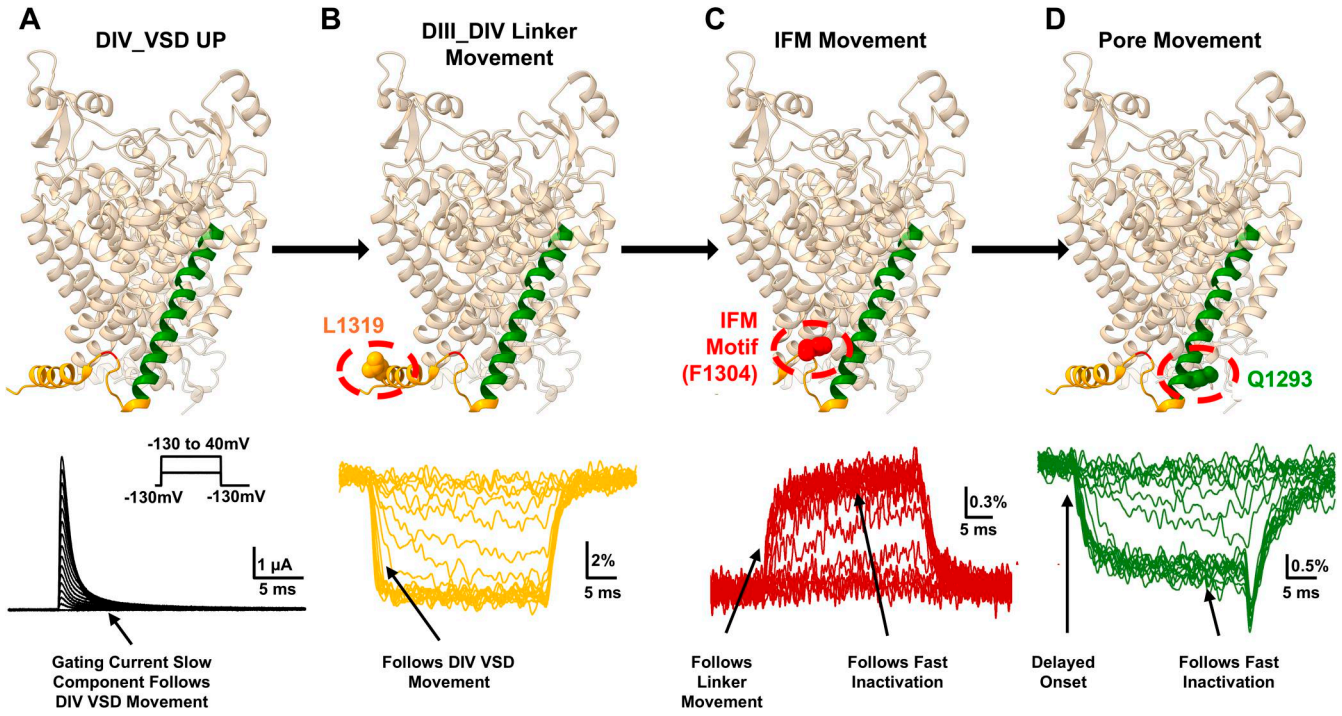

Figure 4. **The IFM motif links DIV VSD activation to inactivation gate. (A)** Upon depolarization, DIV VSD (not shown for simplicity) activates and due to its slow kinetics, manifests as the slow component in the gating current. **(B)** Activation of DIV VSD triggers the DIII–DIV linker (in yellow) movement that attaches via hydrogen bonds, creating a fast decrease in ANAP fluorescence signal (L1319ANAP), suggesting a transition to more hydrophilic environment. This movement is faster than fast inactivation and follows the time course of the DIV VSD movement. **(C)** Movement of the linker is concomitant with the fast movement of the IFM motif (in red, F1304ANAP) that produces the fast component of the increase in fluorescence (more hydrophobic) of the F1304ANAP signal. Subsequently, a second, slower increase of F1304ANAP fluorescence occurs that has the same time constant as the fast inactivation. The increase in the fluorescence signal is also consistent with the notion of IFM motif binding to a hydrophobic pocket. **(D)** DIII S6 closure (in green, Q1293ANAP) tracks the fast inactivation state and occurs with a delayed On, similar to what was observed in the pronase-treated giant squid axon (modified from Liu et al., 2025).

Fig. 4. The activation of the DIV (the slow component of the gating current) triggers the movement of the DIII–DIV linker, in which the IFM motif resides. The movement of the linker positions the IFM motif close to the S6 helices in DIII and DIV, and the IFM motif subsequently triggers a second conformational change at the pore that closes the inactivation gate. In this view, the IFM motif serves as a transducer that couples the activation of DIV VSD to the closure of the inactivation gate located in the S6 transmembrane domains III and IV.

A new fast inactivation model: The lock and key model

Given the close relationships among DIV VSD, the DIII–DIV linker, the IFM motif, and the inactivation gate, interactions must exist to couple these structural components during the fast inactivation process (Fig. 5 A). Based on structural results, two pairs of hydrogen bonds were identified between DIV S4–S5 linker and DIII–DIV linker, one with the phenylalanine in the IFM motif and the other with a downstream glutamine in the linker. Interestingly, in both cases, the carbonyl groups in the protein backbone serve as the hydrogen receivers. Disruptions to these hydrogen bonds lead to impaired fast inactivation (Fig. 5 B) and slowed DIII–DIV linker movement as measured by ANAP fluorescence. It should be pointed out here that these observations support the idea that these hydrogen bonds constitute the driving force for the binding of the IFM motif, and these interactions fix the position of the S4–S5 linker of DIV, thus explaining the immobilization of the charge contributed by the S4 segment of DIV. The backbone nature of the hydrogen bonds also explains why the IQM mutant, a side chain mutation that removes most of the inactivation, still shows half of the charge immobilization, as the VSD of domain IV is still expected to be immobilized.

Mutagenesis experiments in the hydrophobic pocket surrounding the IFM motif identified two key residues for the coupling between the IFM motif and the inactivation gate at the pore. A phenylalanine in DIII S6 and an isoleucine in DIV S6 seem (Fig. 5 C) to be responsible for the coupling between the IFM motif and the inactivation gate. Single alanine replacements of either of the two key hydrophobic residues removed most of the fast inactivation, and a double alanine replacement removed the fast inactivation completely (Fig. 5 C). Abolishing these interactions removed the second, slower movement of the IFM motif during fast inactivation while maintaining the fast movement, as was shown by the ANAP experiment. This result confirms that the identified residues were involved only in transducing the IFM motif's movement to the pore, without impeding the binding of the IFM motif itself. The interactions seemed to depend on both hydrophobic and aromatic interactions. The IFM motif appeared to form a T-shaped pi–pi interaction with the phenylalanine in DIII

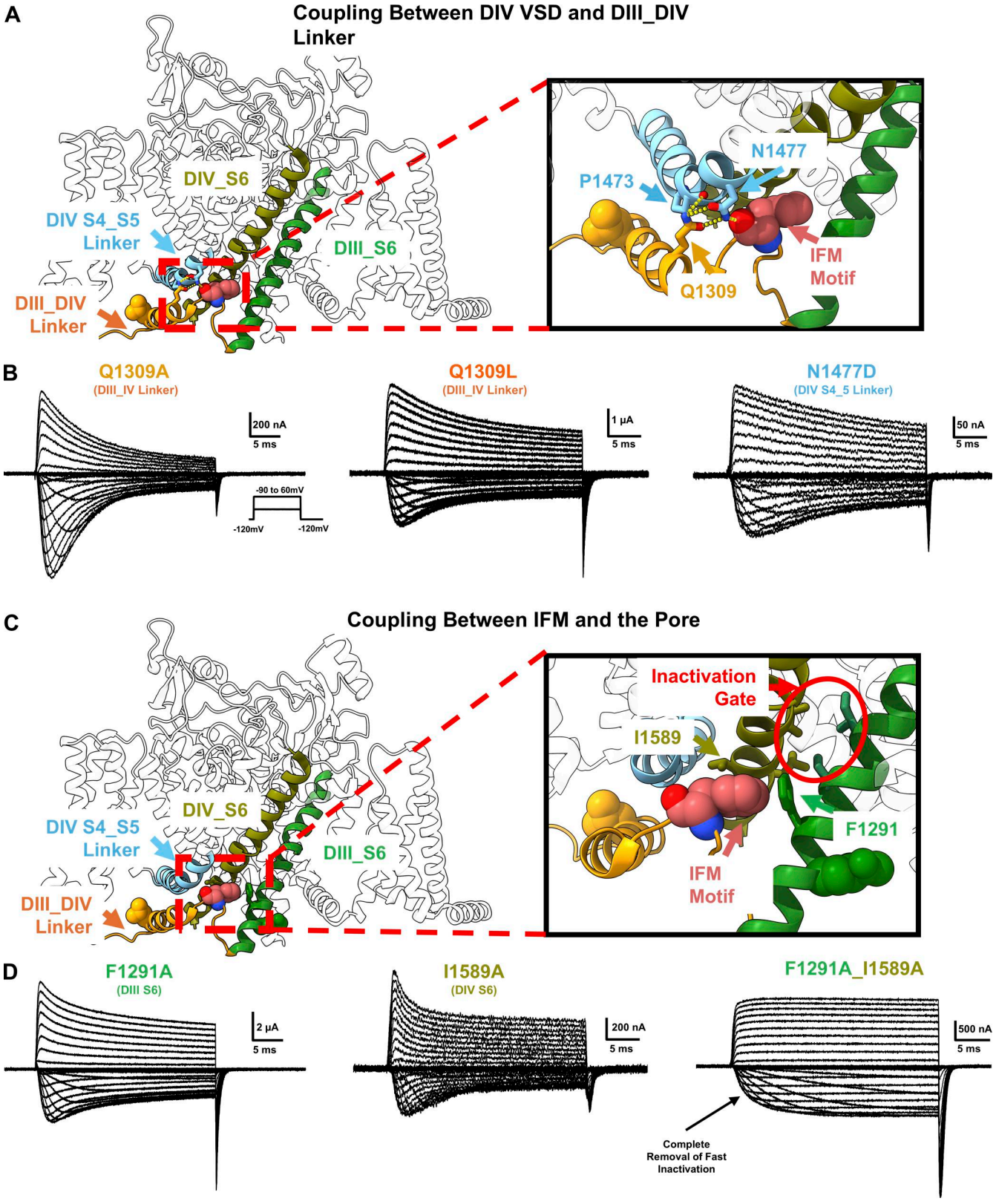

Figure 5. **Structural components and interactions involved in fast inactivation. (A)** Hydrogen bonds couple the DIV VSD and DIII–DIV linker movements. Two hydrogen bonds are identified: N1477 (DIV S4–S5 linker, in orange) with F1304 (IFM motif, in rose), P1473 (DIV S4–S5 linker) with Q1309 (DIII–DIV linker). **(B)** Removal of the hydrogen bonds (Q1309A, Q1309L, and N1477D) leads to severely impaired fast inactivation. **(C)** IFM motif and pore region are coupled through aromatic and hydrophobic interaction. F1291 (DIII S6, in green) forms a t-shaped pi–pi VSD interaction with F1304 (IFM motif) and I1589 (DIV S6, in olive) forms a hydrophobic interaction with IFM motif. **(D)** F1291A and I1589A lead to severe impairment in fast inactivation, and when both are simultaneously mutated, the inactivation is completely removed. Modified from Liu et al. (2025).

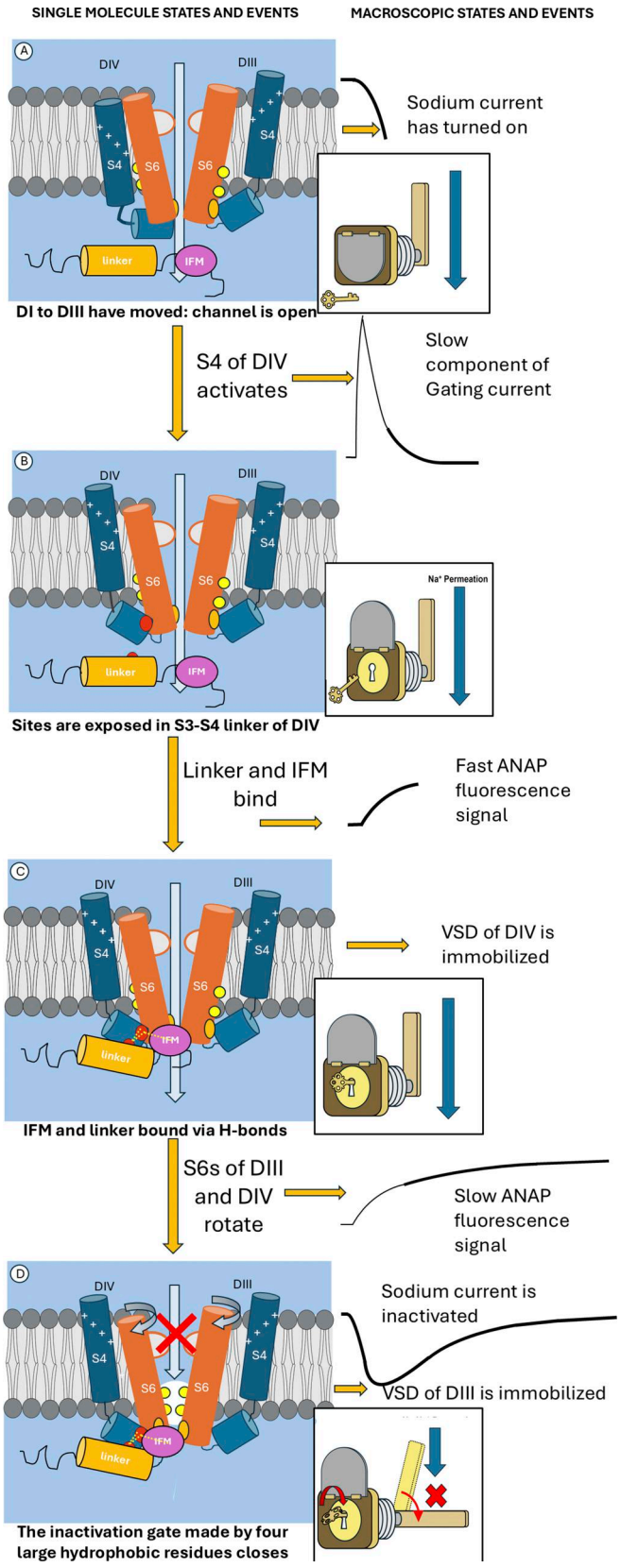

Figure 6. **States and events that lead to inactivation: the lock and key model. (A)** This sequence starts after the VSDs of the first three domains have moved and the channel has opened, as indicated by the early part of the inward Na current (the lock is blocked). Then the VSD of DIV moves, leading to the slow component of the gating current. **(B)** The site in the S3–S4 linker of DIV is exposed, enabling the binding of the IFM motif. (The lock is exposed). The movement of IFM follows that of S4 of DIV, and it is shown as the fast ANAP signal recorded when ANAP replaces the F of the IFM. **(C)** IFM is bound via two pairs of H-bonds, producing the immobilization of the charge of domain IV. (Key is in the lock). With the IFM in position, a rotation of S6 segments of DIII and DIV stabilizes both S6 segments with the phenylalanine in DIII and the isoleucine in domain IV (in orange) by contacting the IFM. If ANAP replaces the F of IFM, this movement generates the slow component of the fluorescence signal. **(D)** The rotation has positioned in the pore all four hydrophobic residues (yellow circles) that form the inactivation gate, thus blocking conduction, shown as the inactivation of the sodium current. At the same time, the contact of the phenylalanine of S6 of DIII with the IFM immobilizes the VSD of DIII. (The lock has rotated and locked).

S6, as the destabilization of this aromatic interaction by fluorinated phenylalanine replacement, which eliminates the T-shaped aromatic interaction, led to incomplete inactivation.

Based on these observations, a lock and key model was proposed. In this view, the fast inactivation apparatus functions as a guarded lock, and the IFM motif serves as the key (Fig. 6 A). Upon depolarization, activation of DIV VSD exposes the binding site for the IFM motif at the DIV S4–S5 linker region, the keyhole (Fig. 6 B). The hydrogen bonds then drive the binding of the IFM motif via backbone interactions, positioning it in a hydrophobic pocket near the S6 helices of DIII and DIV (Fig. 6 C). This is analogous to putting a key inside the keyhole. Once in position, the phenylalanine in the IFM motif likely triggers a rotation of both S6 helices that is stabilized by the two key residues in S6's of DIII and DIV with the IFM, while the rotation moves the hydrophobic inactivation gate into the pore, closing the sodium permeation, like turning the key and locking the lock (Fig. 6 D). The closure of the gate is not expected to be very voltage dependent as the residues are uncharged and moving in a region with a low electric field. In terms of gating charges, the charge immobilization occurs in two separate steps as well. While DIV VSD immobilization is initiated by the initial IFM motif binding, as explained above, DIII VSD immobilization is triggered by the closure of the inactivation gate, which locks S6 of DIII, which is attached via the S3–S4 linker to S4 of DIII.

Future direction of fast inactivation studies in Nav channels

While the new lock and key model reconciles the structural and functional results, many unknowns remain regarding fast inactivation in Nav channels. We would like to briefly discuss some of these open questions with the hope of encouraging further research into the matter.

Connection between the activation gate and the inactivation gate

The bundle crossing region of the intracellular ends of the S6 helices has long been hypothesized to be the activation gate of Nav channels. However, at least in the DIII and DIV cases, the residues seem to be more involved in fast inactivation instead of activation. Structurally, assigning the fast inactivation to the S6 region casts doubt on the location of the activation gate in the

channel. Furthermore, in addition to the open-inactivated state, the closed-inactivated state, which plays several key roles in excitability, also exists (Armstrong, 2006). Intriguingly, structural results seem to suggest that the pores are similar in the closed- and open-inactivated state. Then the transition from the closed to the closed-inactivated state must involve some form of "gate switching" from the activation gate to the inactivation gate. It is not entirely clear how this process occurs and what type of structural rearrangements are involved. However, a possible explanation is based on the fact that, as the movement of VSD in DIV initiates inactivation, it is statistically likely that occasionally the VSD of DIV, although slower, may move before all the other three VSD's have moved in the active position so that, in that case, inactivation will occur before activation.

Resting conformation of the IFM motif and the role of the C terminus

Thus far, almost all structures have been captured in some type of inactivated state. It is unclear what conformation the DIII–DIV linker would adopt in the non-inactivated state. While some argue that the DIII–DIV linker is freely floating in the non-inactivated state, others say that the linker is interacting and is "held" by the C terminus of the channel. Biochemical studies demonstrated that the linker could interact with the C terminus, and C terminus swapping experiments among different isoforms of Nav channels have shown the importance of C termini for fast inactivation (Mantegazza et al., 2001; Chagot et al., 2009; Clairfeuille et al., 2019; Sizova et al., 2020). Clearly, the C terminus is involved in the fast inactivation process and most likely interacts with the non-bound DIII–DIV linker (Goodchild and Ahern, 2024). However, it is difficult due to the lack of a closed-state structure of the Nav channel to determine the exact role of the C terminus and the conformation of the unbound DIII–DIV linker. Additionally, the C terminus likely functions as a hotspot for interactions with other protein regulators (Goldfarb 2011).

Allosteric coupling between fast inactivation and the SF

One unexplained result from DIIIAA and DIVAA is the change in ion selectivity in the leaky inactivated state. It is not clear why the channels become less selective in that state. One possibility is that, as fast inactivation occurs, likely involving rotational movements at S6 in DIII and DIV, the SF is also influenced by conformational changes at the inactivation gate and undergoes rearrangements. In other words, there may be an allosteric coupling between the SF and the fast inactivation gate. Some older TTX/STX studies that demonstrated a use-dependent effect of the toxin at low concentrations support this notion (Salgado et al., 1986; Huang et al., 2012). However, without further experiments, it is difficult to state definitively whether such a connection exists or whether the observed change in selectivity is specific to the mutants.

Interactions between fast and slow inactivation

In addition to the fast inactivation process discussed here, Nav channels undergo a slower, perhaps more complex slow inactivation process. While it is broadly accepted that, as in their K^+ channel counterparts, slow inactivation in Nav channels involves structural rearrangements near the SF region (Yang et al., 1997; Vilin and Ruben, 2001; Silva, 2014; Tan et al., 2022), the exact mechanism remains elusive. However, numerous studies have shown that the fast inactivation process competes with the slow inactivation process. Fast-inactivation–deficient mutants always seem to be able to enter the slow inactivated state faster and more completely (Featherstone et al., 1996). The interaction between fast and slow inactivation is largely unknown, and further exploration is necessary. It is possible that the potential allosteric coupling between fast inactivation and the SF acts as the bridge between these two processes.

Final remarks

Ever since the first description of voltage-dependent sodium current by Hodgkin and Huxley utilizing the voltage-clamp technique, fast inactivation has been a focus of Nav channel studies. Our understanding of fast inactivation mechanisms evolved with the development of new techniques. Gating current measurements with improved electronic equipment enabled the conceptualization of the ball and chain model, and later advancements in cloning and molecular biology prompted the identification of the IFM motif. Biochemical purification of pure toxins revealed key insights into the importance of DIV VSD in fast inactivation, insights subsequently confirmed by voltage-clamp fluorimetry. And all interpretations of the fast inactivation mechanism were revolutionized by high-resolution protein structures obtained through improved cryo-EM. Then, an improved incorporation method for fluorescent unnatural amino acids and enhanced fluorescence measurements once again united the structural data and the functional results, offering a general model for the fast inactivation mechanism. Given the importance of the Nav channel in human physiology and pharmacology, we expect our understanding of fast inactivation to deepen further with ongoing research. With future breakthroughs in measurement techniques, it will be possible to describe the process in full molecular detail.

Acknowledgments

Teresa Giraldez served as editor.

This work was supported by the Chilean government through Fondo Nacional de Desarrollo Científico y Tecnológico Regular #1230265 (R. Latorre), the National Institute Award RO1GM030376 (F. Bezanilla and R. Latorre), National Science Foundation Award QuBBE QLCI (NSF OMA-2121044, F. Bezanilla), and Agencia Nacional de Investigación y Desarrollo Millennium Science Initiative Program, Proyecto ICN2025_026CINV.

Author contributions: Yichen Liu: conceptualization, visualization, and writing—original draft, review, and editing. Cesar A. Amaya-Rodriguez: conceptualization, investigation, methodology, visualization, and writing—original draft, review, and editing. Victoria Collio: conceptualization, investigation, and writing—original draft. Gabriel Ibañez: writing—original draft, review, and editing. Ramón Latorre: conceptualization, methodology, supervision, and writing—review and editing. Francisco

Bezanilla: conceptualization, supervision, validation, visualization, and writing—original draft, review, and editing.

Disclosures: The authors declare no competing interests exist.

Submitted: 11 February 2026
Revised: 24 March 2026
Accepted: 7 April 2026

References

Agnew, W.S., S.R. Levinson, J.S. Brabson, and M.A. Raftery. 1978. Purification of the tetrodotoxin-binding component associated with the voltage-sensitive sodium channel from electrophorus electricus electroplax membranes. *Proc. Natl. Acad. Sci. USA*. 75:2606–2610. https://doi.org/10.1073/pnas.75.6.2606

Aldrich, R.W., D.P. Corey, and C.F. Stevens. 1983. A reinterpretation of mammalian sodium channel gating based on single channel recording. *Nature*. 306:436–441. https://doi.org/10.1038/306436a0

Aman, T.K., and I.M. Raman. 2024. Resurgent current in context: Insights from the structure and function of Na and K channels. *Biophys. J.* 123:1924–1941. https://doi.org/10.1016/j.bpj.2023.12.016

Armstrong, C.M. 1971. Interaction of tetraethylammonium ion derivatives with the potassium channels of giant axons. *J. Gen. Physiol.* 58:413–437. https://doi.org/10.1085/jgp.58.4.413

Armstrong, C.M. 2006. Na channel inactivation from open and closed states. *Proc. Natl. Acad. Sci. USA*. 103:17991–17996. https://doi.org/10.1073/pnas.0607603103

Armstrong, C.M., and F. Bezanilla. 1977. Inactivation of the sodium channel. II. Gating current experiments. *J. Gen. Physiol.* 70:567–590. https://doi.org/10.1085/jgp.70.5.567

Armstrong, C.M., F. Bezanilla, and E. Rojas. 1973. Destruction of sodium conductance inactivation in squid axons perfused with pronase. *J. Gen. Physiol.* 62:375–391. https://doi.org/10.1085/jgp.62.4.375

Armstrong, C.M., and R.S. Croop. 1982. Simulation of Na channel inactivation by thiazine dyes. *J. Gen. Physiol.* 80:641–662. https://doi.org/10.1085/jgp.80.5.641

Bezanilla, F., and C.M. Armstrong. 1977. Inactivation of the sodium channel. I. Sodium current experiments. *J. Gen. Physiol.* 70:549–566. https://doi.org/10.1085/jgp.70.5.549

Campos, F.V., B. Chanda, P.S.L. Beirão, and F. Bezanilla. 2008. Alpha-scorpion toxin impairs a conformational change that leads to fast inactivation of muscle sodium channels. *J. Gen. Physiol.* 132:251–263. https://doi.org/10.1085/jgp.200809995

Capes, D.L., M.P. Goldschen-Ohm, M. Arcisio-Miranda, F. Bezanilla, and B. Chanda. 2013. Domain IV voltage-sensor movement is both sufficient and rate limiting for fast inactivation in sodium channels. *J. Gen. Physiol.* 142:101–112. https://doi.org/10.1085/jgp.201310998

Cha, A., P.C. Ruben, A.L. George Jr, E. Fujimoto, and F. Bezanilla. 1999. Voltage sensors in domains III and IV, but not I and II, are immobilized by Na+ channel fast inactivation. *Neuron*. 22:73–87. https://doi.org/10.1016/s0896-6273(00)80680-7

Cha, A., and F. Bezanilla. 1997. Characterizing voltage-dependent conformational changes in the shaker K+ channel with fluorescence. *Neuron*. 19:1127–1140. https://doi.org/10.1016/s0896-6273(00)80403-1

Cha, A., and F. Bezanilla. 1998. Structural implications of fluorescence quenching in the shaker K+ channel. *J. Gen. Physiol.* 112:391–408. https://doi.org/10.1085/jgp.112.4.391

Chagot, B., F. Potet, J.R. Balser, and W.J. Chazin. 2009. Solution NMR structure of the C-terminal EF-hand domain of human cardiac sodium channel NaV1.5. *J. Biol. Chem.* 284:6436–6445. https://doi.org/10.1074/jbc.M807747200

Chanda, B., and F. Bezanilla. 2002. Tracking voltage-dependent conformational changes in skeletal muscle sodium channel during activation. *J. Gen. Physiol.* 120:629–645. https://doi.org/10.1085/jgp.20028679

Chatterjee, A., J. Guo, H.S. Lee, and P.G. Schultz. 2013. A genetically encoded fluorescent probe in mammalian cells. *J. Am. Chem. Soc.* 135:12540–12543. https://doi.org/10.1021/ja4059553

Clairfeuille, T., A. Cloake, D.T. Infield, J.P. Llongueras, C.P. Arthur, Z.R. Li, Y. Jian, M.F. Martin-Eauclaire, P.E. Bougis, C. Ciferri, et al. 2019. Structural basis of a-scorpion toxin action on Na v channels. *Science*. 363:eaav8573. https://doi.org/10.1126/science.aav8573

Correa, A.M., F. Bezanilla, and W.S. Agnew. 1990. Voltage activation of purified eel sodium channels reconstituted into artificial liposomes. *Biochemistry*. 29:6230–6240. https://doi.org/10.1021/bi00478a017

Correa, A.M., R. Latorre, and F. Bezanilla. 1991. Ion permeation in normal and batrachotoxin-modified Na+ channels in the squid giant axon. *J. Gen. Physiol.* 97:605–625. https://doi.org/10.1085/jgp.97.3.605

Eaholtz, G., T. Scheuer, and W.A. Catterall. 1994. Restoration of inactivation and block of open sodium channels by an inactivation gate peptide. *Neuron*. 12:1041–1048. https://doi.org/10.1016/0896-6273(94)90312-3

Featherstone, D.E., J.E. Richmond, and P.C. Ruben. 1996. Interaction between fast and slow inactivation in Skm1 sodium channels. *Biophys. J.* 71:3098–3109. https://doi.org/10.1016/s0006-3495(96)79504-8

Goldfarb, M. 2011. Voltage-gated sodium channel-associated proteins and alternative mechanisms of inactivation and block. *Cell Mol. Life Sci.* 69:1067–1076. https://doi.org/10.1007/s00018-011-0832-1

Goodchild, S.J., and C.A. Ahern. 2024. Conformational photo-trapping in NaV1.5: Inferring local motions at the 'inactivation gate'. *Biophys. J.* 123:2167–2175. https://doi.org/10.1016/j.bpj.2024.04.017

Hanck, D.A., and M.F. Sheets. 2006. Site-3 toxins and cardiac sodium channels. *Toxicon*. 49:181–193. https://doi.org/10.1016/j.toxicon.2006.09.017

Hille, B. 1970. Ionic channels in nerve membranes. *Prog. Biophys. Mol. Biol.* 21:1–32. https://doi.org/10.1016/0079-6107(70)90022-2

Hille, B. 1971. The permeability of the sodium channel to organic cations in myelinated nerve. *J. Gen. Physiol.* 58:599–619. https://doi.org/10.1085/jgp.58.6.599

Hille, B. 1973. Potassium channels in myelinated nerve selective permeability to small cations. *J. Gen. Physiol.* 61:669–686. https://doi.org/10.1085/jgp.61.6.669

Hodgkin, A.L., and A.F. Huxley. 1952a. A quantitative description of membrane current and its application to conduction and excitation in nerve. *J. Physiol.* 117:500–544. https://doi.org/10.1113/jphysiol.1952.sp004764

Hodgkin, A.L., and A.F. Huxley. 1952b. Currents carried by sodium and potassium ions through the membrane of the giant axon of Loligo. *J. Physiol.* 116:449–472. https://doi.org/10.1113/jphysiol.1952.sp004717

Hodgkin, A.L., and A.F. Huxley. 1952c. The components of membrane conductance in the giant axon of Loligo. *J. Physiol.* 116:473–496. https://doi.org/10.1113/jphysiol.1952.sp004718

Hodgkin, A.L., and A.F. Huxley. 1952d. The dual effect of membrane potential on sodium conductance in the giant axon of Loligo. *J. Physiol.* 116:497–506. https://doi.org/10.1113/jphysiol.1952.sp004719

Hodgkin, A.L., A.F. Huxley, and B. Katz. 1952. Measurement of current-voltage relations in the membrane of the giant axon of Loligo. *J. Physiol.* 116:424–448. https://doi.org/10.1113/jphysiol.1952.sp004716

Hodgkin, A.L., and R.D. Keynes. 1955. The potassium permeability of a giant nerve fibre. *J. Physiol.* 128:61–88. https://doi.org/10.1113/jphysiol.1955.sp005291

Hoshi, T., W.N. Zagotta, and R.W. Aldrich. 1990. Biophysical and molecular mechanisms of shaker potassium channel inactivation. *Science*. 250:533–538. https://doi.org/10.1126/science.2122519

Huang, C.J., L. Schild, and E.G. Moczydlowski. 2012. Use-dependent block of the voltage-gated Na(+) channel by tetrodotoxin and saxitoxin: Effect of pore mutations that change ionic selectivity. *J. Gen. Physiol.* 140:435–454. https://doi.org/10.1085/jgp.201210853

Jiang, D., H. Shi, L. Tonggu, T.M. Gamal El-Din, M.J. Lenaeus, Y. Zhao, C. Yoshioka, N. Zheng, and W.A. Catterall. 2020. Structure of the cardiac sodium channel. *Cell*. 180:122–134.e10. https://doi.org/10.1016/j.cell.2019.11.041

Jiang, D., R. Banh, T.M. Gamal El-Din, L. Tonggu, M.J. Lenaeus, R. Pomès, N. Zheng, and W.A. Catterall. 2021. Open-state structure and pore gating mechanism of the cardiac sodium channel. *Cell*. 184:5151–5162.e11. https://doi.org/10.1016/j.cell.2021.08.021

Kuo, C.C., and B.P. Bean. 1994. Na+ channels must deactivate to recover from inactivation. *Neuron*. 12:819–829. https://doi.org/10.1016/0896-6273(94)90335-2

Liu, Y., C.A.Z. Bassetto Jr, B.I. Pinto, and F. Bezanilla. 2023. A mechanistic reinterpretation of fast inactivation in voltage-gated Na+ channels. *Nat. Commun.* 14:1–13. https://doi.org/10.1038/s41467-023-40514-4

Liu, Y., J.D. Galpin, C.A. Ahern, and F. Bezanilla. 2025. Molecular basis of sodium channel inactivation. *Nat. Commun.* 16:10565. https://doi.org/10.1038/s41467-025-65587-1

Mannuzzu, L.M., M.M. Moronne, and E.Y. Isacoff. 1996. Direct physical measure of conformational rearrangement underlying potassium channel gating. *Science*. 271:213–216. https://doi.org/10.1126/science.271.5246.213

Mantegazza, M., F.H. Yu, W.A. Catterall, and T. Scheuer. 2001. Role of the C-terminal domain in inactivation of brain and cardiac sodium

channels. *Proc. Natl. Acad. Sci. USA*. 98:15348–15353. https://doi.org/10.1073/pnas.211563298

Neher, E., and B. Sakmann. 1976. Single-channel currents recorded from membrane of denervated frog muscle fibres. *Nature*. 260:799–802. https://doi.org/10.1038/260799a0

Noda, M., S. Shimizu, T. Tanabe, T. Takai, T. Kayano, T. Ikeda, H. Takahashi, H. Nakayama, Y. Kanaoka, and N. Minamino. 1984. Primary structure of electrophorus electricus sodium channel deduced from cDNA sequence. *Nature*. 312:121–127. https://doi.org/10.1038/312121a0

Noda, M., T. Ikeda, H. Suzuki, H. Takeshima, T. Takahashi, M. Kuno, and S. Numa. 1986. Expression of functional sodium channels from cloned cDNA. *Nature*. 322:826–828. https://doi.org/10.1038/322826a0

Pan, X., Z. Li, Q. Zhou, H. Shen, K. Wu, X. Huang, J. Chen, J. Zhang, X. Zhu, J. Lei, et al. 2018. Structure of the human voltage-gated sodium channel Nav1.4 in complex with β1. *Science*. 362:eaau2486. https://doi.org/10.1126/science.aau2486

Patton, D.E., J.W. West, W.A. Catterall, and A.L. Goldin. 1993. A peptide segment critical for sodium channel inactivation functions as an inactivation gate in a potassium channel. *Neuron*. 11:967–974. https://doi.org/10.1016/0896-6273(93)90125-B

Rogers, J.C., Y. Qu, T.N. Tanada, T. Scheuer, and W.A. Catterall. 1996. Molecular determinants of high affinity binding of α-scorpion toxin and sea anemone toxin in the S3-S4 extracellular loop in domain IV of the Na+ channel α subunit. *J. Biol. Chem.* 271:15950–15962. https://doi.org/10.1074/jbc.271.27.15950

Rojas, E., and M. Luxoro. 1963. Micro-injection of trypsin into axons of squid. *Nature*. 199:78–79. https://doi.org/10.1038/199078b0

Rosenberg, R.L., S.A. Tomiko, and W.S. Agnew. 1984. Single-channel properties of the reconstituted voltage-regulated Na channel isolated from the electroplax of electrophorus electricus. *Proc. Natl. Acad. Sci. USA*. 81:5594–5598. https://doi.org/10.1073/pnas.81.17.5594

Salgado, V.L., J.Z. Yeh, and T. Narahashi. 1986. Use- and voltage-dependent block of the sodium channel by saxitoxin. *Ann. N. Y. Acad. Sci.* 479:84–95. https://doi.org/10.1111/j.1749-6632.1986.tb15563.x

Silva, J. 2014. Slow Inactivation of Na+ Channels. *In* Handbook of Experimental Pharmacology. Vol. 221. Springer, Berlin, Heidelberg. 33–49.

Sizova, D.V., J. Huang, E.J. Akin, M. Estacion, C. Gomis-Perez, S.G. Waxman, and S.D. Dib-Hajj. 2020. A 49-residue sequence motif in the C terminus of Nav1.9 regulates trafficking of the channel to the plasma membrane. *J. Biol. Chem.* 295:1077–1090. https://doi.org/10.1074/jbc.RA119.011424

Stevens, M., S. Peigneur, and J. Tytgat. 2011. Neurotoxins and their binding areas on voltage-gated sodium channels. *Front. Pharmacol.* 2:14152. https://doi.org/10.3389/fphar.2011.00071

Stimers, J.R., F. Bezanilla, and R.E. Taylor. 1985. Sodium channel activation in the squid giant axon. Steady state properties. *J. Gen. Physiol.* 85:65–82. https://doi.org/10.1085/jgp.85.1.65

Stühmer, W., F. Conti, H. Suzuki, X.D. Wang, M. Noda, N. Yahagi, H. Kubo, and S. Numa. 1989. Structural parts involved in activation and inactivation of the sodium channel. *Nature*. 339:597–603. https://doi.org/10.1038/339597a0

Tan, X.F., C. Bae, R. Stix, A.I. Fernández-Mariño, K. Huffer, T.-H. Chang, J. Jiang, J.D. Faraldo-Gómez, andK.J. Swartz. 2022. Structure of the shaker Kv channel and mechanism of slow C-type inactivation. *Sci. Adv.* 8:eabm7814. https://doi.org/10.1126/sciadv.abm7814

Tang, L., R.G. Kallen, and R. Horn. 1996. Role of an S4-S5 linker in sodium channel inactivation probed by mutagenesis and a peptide blocker. *J. Gen. Physiol.* 108:89–104. https://doi.org/10.1085/jgp.108.2.89

Tonggu, L., G. Wisedchaisri, T.M. Gamal El-Din, M.J. Lenaeus, M.M. Logan, T. Toma, J. Du Bois, N. Zheng, and W.A. Catterall. 2024. Dual receptor-sites reveal the structural basis for hyperactivation of sodium channels by poison-dart toxin batrachotoxin. *Nat. Commun.* 15:2306. https://doi.org/10.1038/s41467-024-45958-w

Ulbricht, W. 2005. Sodium channel inactivation: Molecular determinants and modulation. *Physiol. Rev.* 85:1271–1301. https://doi.org/10.1152/physrev.00024.2004

Vandenberg, C.A., and F. Bezanilla. 1991. A sodium channel gating model based on single channel, macroscopic ionic, and gating currents in the squid giant axon. *Biophys. J.* 60:1511–1533. https://doi.org/10.1016/S0006-3495(91)82186-5

Vassilev, P.M., T. Scheuer, and W.A. Catterall. 1988. Identification of an intracellular peptide segment involved in sodium channel inactivation. *Science*. 241:1658–1661. https://doi.org/10.1126/science.2458625

Vilin, Y.Y., and P.C. Ruben. 2001. Slow inactivation in voltage-gated sodium channels: Molecular substrates and contributions to channelopathies. *Cell Biochem. Biophys.* 35:171–190. https://doi.org/10.1385/CBB:35:2:171

Wang, S.Y., K. Bonner, C. Russell, and G.K. Wang. 2003. Tryptophan scanning of D1S6 and D4S6 C-termini in voltage-gated sodium channels. *Biophys. J.* 85:911–920. https://doi.org/10.1016/S0006-3495(03)74530-5

Wang, S.Y., and G.K. Wang. 2005. Block of inactivation-deficient cardiac Na(+) channels by acetyl-KIFMK-amide. *Biochem. Biophys. Res. Commun.* 329:780–788. https://doi.org/10.1016/j.bbrc.2005.02.039

Weber, G., and F.J. Farris. 1979. Synthesis and spectral properties of a hydrophobic fluorescent probe: 6-Propionyl-2 (dimethylamino)naphthalene. *Biochemistry*. 18:3075–3078. https://doi.org/10.1021/bi00581a025

West, J.W., D.E. Patton, T. Scheuer, Y. Wang, A.L. Goldin, and W.A. Catterall. 1992. A cluster of hydrophobic amino acid residues required for fast Na(+)-channel inactivation. *Proc. Natl. Acad. Sci. USA*. 89:10910–10914. https://doi.org/10.1073/PNAS.89.22.10910

Yan, Z., Q. Zhou, L. Wang, J. Wu, Y. Zhao, G. Huang, W. Peng, H. Shen, J. Lei, and N. Yan. 2017. Structure of the Nav1.4-β1 complex from electric eel. *Cell* 170:470–482.e11. https://doi.org/10.1016/j.cell.2017.06.039

Yang, Y., Y. Yan, and F.J. Sigworth. 1997. How does the W434F mutation block current in Shaker potassium channels? *J. Gen. Physiol.* 109:779–789. https://doi.org/10.1085/JGP.109.6.779

Yarov-Yarovoy, V., J.C. McPhee, D. Idsvoog, C. Pate, T. Scheuer, and W.A Catterall. 2002. Role of amino acid residues in transmembrane segments IS6 and IIS6 of the Na+ channel α subunit in voltage-dependent gating and drug block. *J. Biol. Chem.* 277:35393–35401. https://doi.org/10.1074/jbc.M206126200

Zhang, J., Y. Shi, J. Fan, H. Chen, Z. Xia, B. Huang, J. Jiang, J. Gong, Z. Huang, and D. Jiang. 2022. N-type fast inactivation of a eukaryotic voltage-gated sodium channel. *Nat. Commun.* 13:1–10. https://doi.org/10.1038/s41467-022-30400-w